## RESEARCH ARTICLE

# Overcoming Conflicts of Objectives Between Sensory and Mechanical Domain in the Development of Sensor-Integrating Machine Elements Using the Example of Bolts

JULIAN PETERS[ID]1, NATHANAEL MIRBACH1, FELIX HERBST[ID]2, (Student Member, IEEE),
DAVID RIEHL[ID]3, (Student Member, IEEE), MARIO KUPNIK[ID]2, (Senior Member, IEEE),
KLAUS HOFMANN[ID]3, (Senior Member, IEEE), AND SVEN MATTHIESEN[ID]1

1Institute of Product Engineering, Karlsruhe Institute of Technology (KIT), 76131 Karlsruhe, Germany
2Measurement and Sensor Technology Group, Technische Universität Darmstadt, 64289 Darmstadt, Germany
3Integrated Electronic Systems Laboratory, Technische Universität Darmstadt, 64289 Darmstadt, Germany

Corresponding author: Julian Peters (julian.peters@kit.edu)

**ABSTRACT** Comprehensive data on machines is essential for digitization in the industry. Since standardized machine elements are used in most machines, integrating them with sensors provides the opportunity to acquire data comprehensively from in-situ. The sensor integration must not change the element's core function and the standardized mechanical interfaces. Hence, sensors must be fully integrated and self-sufficient. Regarding bolts as widely used machine element, a solution that combines all the aforementioned requirements does not yet exist. A main problem in developing sensor-integrating machine elements and especially bolts is to overcome the conflicting objectives in defining design space for mechanical and sensory functions. There is a lack of an approach to model the effects of the design space parameters on the mechanical and sensory functions. This paper proposes an optimization function to aid mechanical and electrical engineers in resolving conflicting objectives by balancing function fulfillment when determining design space parameters. Therefore, the effects of the parameters on the mechanical and sensory functions are modelled using FE-analysis and composing an optimization function with weights. This function provides optimal design space parameters. With respect to mountability boundary conditions the optimum for equal weights is at diameters 13.2 mm both, increasing v. Mises stress by 29% and strain at sensor position by 80%. The location of the optimum is very dependent on proper weighting, which resembles a prioritization of the mechanical versus the sensory function fulfillment. This enables engineers to find optimal parameters by balancing the mechanical and the sensory function fulfillment.

**INDEX TERMS** Bolt, conflicting objectives, design space, finite element analysis, mechanical domain, optimization, sensing, sensor, sensory domain, sensor integration, strain gauges.

## I. INTRODUCTION

In the era of digitization, the utilization of data to improve performance is focused. This underlines the importance of comprehensively gathering data with widespread sensor

The associate editor coordinating the review of this manuscript and approving it for publication was Frederico Guimarães[ID].

technologies [1]. The benefits of condition monitoring (CM) and structural health monitoring (SHM) are based on comprehensively acquired data, enabling the interpretation of a machine's or plant's condition and thus its optimization [2], [3], [4], [5]. In particular, in-situ data at process-relevant locations can provide deep insight and reliable interpretations on the state of health and the processes, as shown in several

works on transmissions, hydraulic systems, manufacturing and additively manufactured parts, for example [6], [7], [8], [9], [10], [11].

Moreover, widespread in-situ data provides a good opportunity to fuel digital twins. These rely on comprehensively modeling the physical world [12], [13]. Sensor data of high quality is needed to adequately parameterize and characterize data-driven models (physical-to-virtual twinning), which in turn can be used to operate predictive maintenance, fault diagnosis, etc. (virtual-to-physical twinning) [12], [13].

However, existing sensor solutions are mostly individually manufactured for a specific system and measurement quantity and hence adaptation to other systems is costly. In other words, there is a lack of compact, autonomous and easy-to-use sensors at reasonable cost that can be installed in-situ [14], [15].

This gap in acquiring comprehensive measurement data can be closed by extending machine elements with measurement capabilities, such as sensing or sensor-integrating machine elements (SiME) [16]. Standardized machine elements are installed in almost every technical system, thus SiME have a huge potential to acquire comprehensive measurement data in-situ.

Classic machine elements are easy to be integrated on system level, due to their standardized interfaces. The sensor integration must not change these mechanical interfaces and the core functionality. Hence, the sensors need to be fully integrated and self-sufficient. Moreover, cable connections must be avoided as they take up additional installation space and make retrofitting more difficult. Hence, electronics to sample and wirelessly transmit the sensor data and an interface for wireless power supply need to be integrated into the machine elements as well. Addressing this topic, a research program (DFG priority program 2305 [17]) was set up by the German Research Foundation (DFG). This contribution is part of the project "Sensor-integrating Bolts for Multi-axial Force Measurement and Deduction of a Design Methodology for Sensor-integration in Closed Cylindrical Machine Elements" within this program.

This work focuses on sensor integration into standardized metric bolts, because they are among the most widespread machine elements [18] and are usually within the force flow [19]. This opens a huge potential to predict system states out of the bolt's measurement data. There are several standards for metric bolts, like the DIN 13-1 [20] specifying the thread, the DIN EN ISO 4014 [21] specifying hexagonal head forms and shafts and the VDI 2230 [22] for the calculation of the loadability of bolts. The sensor-integrating bolt must comply with these standards to ensure widespread usability and retrofitting.

Bolts usually bear multi-axial loads [19]. When bolts are tightened conventionally, the torsional torque is superimposed with tensile forces. Additional tensile forces and bending torques can occur during operation [23]. This makes multi-axial measurement necessary to fully measure the bolt's state.

In summary, the requirements needing to be fulfilled are to:

- maintain the mechanical function,
- keep the standardized mechanical interfaces (head, thread, outer diameters),
- prevent wire bound energy supply or communication, as this prevents easy integration,
- provide measurement for all relevant load cases (for bolts multi-axial, referring to [23]).

Furthermore, developing SiME is challenging not only because of the strict requirements as mentioned above, but also because of the involvement of various disciplines such as mechanics, electronics, and information technology that share the same design parameters [24]. In most cases, the integration of the sensors disrupts the original structure [25], meaning the mechanical function. This often leads to conflicts in the development [26] and requires trade-offs.

Kirchner et al. [14] also mention the need for models and methods to balance the mechanical and sensory functions of the solutions to support the engineers of the involved disciplines to negotiate efficiently for their functions. This gap the solution presented in this paper intends to fill.

The state-of-the-art shows numerous examples of the challenges to integrate sensing functions while trying to maintain the mechanical functions.

### A. STATE-OF-THE-ART

Force-measuring bolts exist, but they have individual disadvantages lined out in detail in the following text. In summary:

- no sufficient sensing functionality exists (only uniaxial measurement),
- the mechanical function is weakened (loss of load capacity),
- the installation conditions are modified (wire bound, change of mechanical interfaces).

The CiS Research Institute for Microsensors in cooperation with the Department of Measurement and Sensor Technology from TU-Darmstadt uses piezoresistive silicon strain gauge elements on the bolt's head to measure the bolt's axial force (no multi-axial measurement was shown) [27]. The sensors and the electronics used to capture and transmit data are mounted externally on the bolt head. This does not reduce the bolt's loadability (mechanical function). However, the outer dimensions on the bolt head are not preserved, interfering with the mechanical interface needed for tools to tighten the bolt.

The Fraunhofer CCIT developed a Smart bolt Connection that addresses energy self-sufficiency via solar cells or thermogenerators [28], [29]. The measuring element is a thin-film sensor system (DiaForce) that is integrated into a washer together with the electronics for data acquisition and wireless transfer on a PCB. Measurements of uni-axial forces are shown (no multi-axial, bending torque measurement) [28]. The installation of sensors and electronics do not harm the mechanical function, however, change the installation

conditions and properties of the whole bolt connection by adding an extra washer and casing on the head.

Groche et al. present a bolt of size M24 integrating a sensor body with strain gauges that is fitted into a cylindrical cavity of a bolt by an incremental forming process [19]. Thread and head are individually machined. The sensor assembly contains three strain gauges (SG), which are applied on three sides of a rectangular cross-section. Theoretically, this would allow measurement of axial forces and bending torques independently. However, the authors do not prove this by tests and measurements. In the M24 bolt (no shaft, thread root diameter 22.05 mm) they have a cavity with diameter of 10 mm. Further, the authors state that the sensitivity of the sensor is proportional to the stiffness of the composite combination of sensor body and the bolt's remaining structure [19]. As the stiffness is dependent on the cross-section area, the sensitivity of the measurement is dependent on this area. This in turn is dependent on the bolt's and cavity's diameter. This dependency will be used to formulate the sensor quality in this contribution. The measurement results of the authors suggest that the sensor body's stiffness adds to the bolt's stiffness, leading to a restrengthening through the sensor body. For evaluating the stiffness, only the thread root diameter is considered, influences of the thread and notches are neglected.

The company ConSenses offers sensor-integrating bolts commercially sold as "PiezoBolts" [30]. A measuring body with piezo-rings for strain measurement are pressed into the bolt, using similar incremental forming process as Brenneis et al. [31] and Groche et al. [19]. This enables uni-axial force measurement. According to the company the mechanical properties are equivalent to the standards of metrical screws (VDI 2230 [22]), the tightening torques and pretension forces match those of bolt strength class 8.8 [32]. Since the bolts are manufactured by the company, no statement to the loss of strength by sensor body cavities can be made. Energy supply and data transmission is wire bound via a plug connection at the bolt head. The PiezoBolts are capable of measuring forces dynamically with a sensitivity of single digit Newtons.

The company CoreSensing offers one of the few integrated sensor systems capable of measuring multi-axial forces (including torques) and providing wireless data transfer [33]. Power is fed by an integrated energy storage, that runs up to one year before needing to be recharged. However, the sensor system is pressed into cavities with inner diameters of 14 mm or more [33], making it usable for big bolts only. The influence of the cavity on the mechanical function needs to be considered closely.

As prior work to this contribution, Herbst et al. [34] presented a sensor system using strain-gauges (SG) for multi-axial force and torque measurement. It is designed for a M20 bolt with a shaft diameter 20 mm needing a cavity of 12 mm for the sensor body with the SGs. According to the authors, this reduces the bolt's loadability (mechanical function) of one material strength class, which is 20%-25%.

Bonaiti et al. analyzes the loadability of a gear for integration of sensors [35]. The methods used by the authors may be transferable to bolts as well. Finite-element (FE) analysis is conducted to evaluate the effect of the cavities for the sensors in the gear on the load bearing capacity (i.e. the mechanical function). In the paper the authors analyze the sensor position and its distance to their point of interest for measurements, the gear meshing, against the reduction of load carrying capacity. The authors modified the body of the gear by introducing cavities to integrate small PCBs with the sensors as close as possible to the gear contact, without unreasonably affecting the load carrying capacity. The authors present three different shapes of the cavities, of which two with easy, annular designs are reasoned as being not-feasible by qualitative considerations and by literature references. The authors then followed the inspiration of lightweight gears to design the cavities. With several iterations in FE simulation they defined design space parameters that reduce the effect on the load carrying capacity, represented by an equivalent mechanical stress. This stress increases up to 22% due to the cavities for the sensors and electronics, therefore reducing the load bearing capacity and thus the mechanical function. The authors conclude that a sensor-integrated gear must sacrifice some of its load carrying capacity to accommodate the additional intelligence in the form of space for sensors. However, the effect of the cavity parameters on the sensory function is not quantified in the cited paper.

Dumstorff et al. present several possibilities to integrate sensors in material in a minimal invasive way, not harming its original properties (i.e. mechanical function) [25]. The authors perform 2D FE analysis on a rectangular bar with a rectangular cavity for sensors (called inlay) that have a different Young's modulo (elastic modulo, E). The bar is subjected to tensile and bending loads. The change of the relative v. Mises stress is observed for different elastic modulo of the inlay. When the inlay is weaker than the surrounding material the stress in the inlay decreases, but the stress at the edges of the outer structure increases. This is comparable to the case of the sensor-integrating bolts regarded in this contribution, where the sensors will have a lower elastic modulo than the bolt's steel surrounding it. The authors conclude that the inlay should have similar elastic properties than the surrounding material for minimal stress increase. This can have a negative effect on the endurance of the electronics though [36].

Kirchner et al. state that models connecting the function to the structure and modifiable parameters are elementary for balancing the mechanical and sensory functions [14] (also called function-behavior-structure models [37], [38], [39]). Providing this, "balanced [sensing] solutions tailored to the individual use-cases of the machine elements" [14] can be achieved.

An overview of the challenges, methods and activities already used in the state of the art of SiME development is described in prior work by the authors of this

contribution [24]: In summary, many sensor-integrating projects share similar challenges. One of the biggest are the **conflicts arising due to different disciplines sharing the same design parameters**. An optimum for one discipline can be a bad solution for another [26].

The authors state that in the state-of-the-art no standardized procedure is found to solve this conflict of objectives regarding SiME. Procedures used are "bottom-up" or "top-down approaches" that either select a sensor and fit it inside the element (prioritize sensory function) or that define a maximum volume and select sensors that fit in (prioritize mechanical function) [24].

### B. PROBLEM SUMMARY AND AIM OF THIS PAPER

The problem in optimizing sensor-integrating bolts is to overcome the conflicting objectives of mechanical and sensory functions in terms of the design space.

The **mechanical function** of a standard bolt is to apply clamping force on two different elements to eliminate relative movement. Without changing the outer dimensions as requested before, the sensors need to be situated inside the screw, which makes cavities necessary. However, this leads to a reduction of material and load capacity, which leads to a reduction of clamping force. Also, the outer shape of the bolt must be maintained to preserve the mechanical interfaces and keep the standards.

The **sensory function** of a sensor-integrating bolt for force measurement is to reliably determine the load condition (i.e. force and torque vector) of the bolt. Therefore, space for sensors and electronics to read out and supply the sensors inside the bolt is required. Also, measurement quality in terms of sensitivity, resolution and accuracy is likely to increase, having more design space for sensors. To a certain degree this is also valid for signal-to-noise ratio and data rate, because having more space for electronics provides more freedom for choosing and placing electronic components.

This leads to the conflict of objectives, the sensory function harms the mechanical function via the design space and vice versa. To overcome this and to decide which function gets how much design space, the effects of the parameters of the design space on the mechanical and sensory functions must be investigated and quantified. The following research question will be investigated with the focus on strain gauges as force sensors:

*How to overcome the conflict of objectives between the mechanical and sensory function fulfillment in identifying optimal design space parameters for force sensors?*

## II. METHODS

This chapter contains the methodical approach to answer the research question. First, a general approach is introduced, which is then applied to the example case of bolts.

The aim is to compose an optimization function (O(DS)) that contains the effect of the design space (DS) parameters for the sensor integration on the mechanical as well as sensory function.
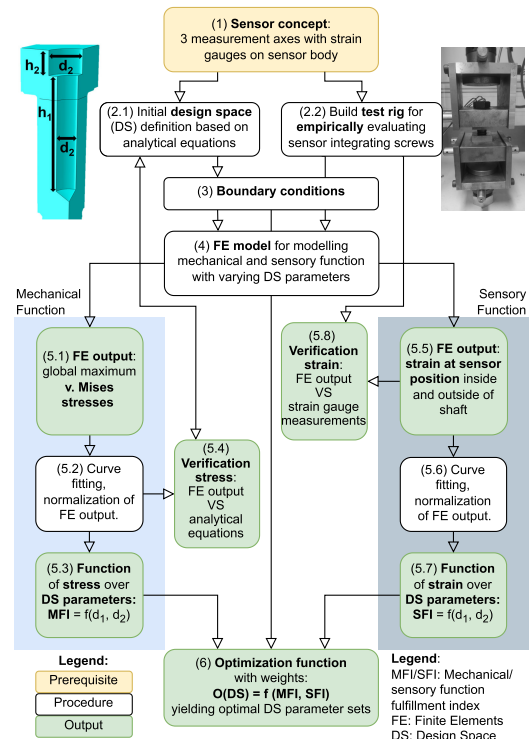


**FIGURE 1.** Overview of the general approach for design space identification by composing an optimization function including models of mechanical and sensory function fulfillment, based on [40].

### A. GENERAL APPROACH

Figure 1 shows the general approach used to compose the optimization function.

A prerequisite for starting the modelling of the effect of the DS parameters on mechanical and sensory function fulfillment, a **sensor concept** (step 1) is needed to define a reasonable idea of an initial **design space** in terms of shape and location (DS parameters) in the bolt, based on the analytical equation for the v. Mises stress (step 2.1). The stress outputs of the equation are used to determine the utilization of the material, hence helps in finding areas for the design space that have lower influences on the mechanical function fulfillment. Reducing calculation effort, the v. Mises equation is formulated in a 2D cross-section of the most critical area, considering the influence of notches on the stress.

To allow empirical testing of the outputs of later steps, a **test rig** for the object under investigation is built (step 2.2). It has the possibility to load the test object with multi-axial forces.

Boundary conditions need to be defined (step 3), concerning maximum loads, interactions, mountability, for example.

Next, a **Finite Elements (FE) model** is set up (step 4). It resembles the test rig of step 2.2 to allow comparison of virtual versus real testing outcomes. The FE model has a fixed load case and is modifiable for design space parameters in shape and location that was determined in step 2.1.

Next, the approach splits into the modelling of the mechanical and sensory function. A DS parameter study is conducted using the FE model. The **FE outputs** of the **v. Mises stress** is used for the **mechanical part** (step 5.1) and the **strain** is used for the **sensory part** (step 5.5). The output data point sets are **curve fitted** to retrieve a function of the stress respectively strain with respect to the DS parameters (steps 5.2, 5.6). The functions are normalized to a maximum value. This results in **mechanical** (5.3) respectively **sensory** (5.7) **fulfillment indices**.

The **verification of the FE stress output** is performed by comparing the normalized global maximum FE outputs to the results of the stress equation from step 2 at the most critical cross-section (step 5.4).

The **verification of the FE strain outputs** is done by comparing the FE strain output at defined points to measurements with strain gauges in the test rig from step (2.2) at the same points.

Finally, the mechanical and the sensory fulfillment indices are combined to a single **optimization function**, with respect to the DS parameters (step 6). If necessary, the function fulfillment indices are inverted to match the function's objective: With the optimum being the minimum, a stress increase means a higher index and a strain increase means a lower index. Weighting factors are introduced to be able to prioritize the mechanical versus the sensory part.

In the following, details to the method steps from Figure 1 are explained in detail. The first step is the initial definition of the design space, explained in secs. II-B and II-C.

## B. SENSOR CONCEPT

A reasonable initial definition of the design space is needed to reduce the solution space to a manageable range. Therefore, a sensor concept needs to be defined (Figure 1 step (1)).

The basic idea of the measurement concept for evaluating multi-axial forces in a bolt is to have at least three measurement axes, that are spaced symmetrically around a circumference in a cross-section of the bolt, as it was shown in prior work [34].

In this work we focus on strain gauges (SG) as transducers. To reliably install SGs it is elementary to have good access to the application area. Installing SGs inside a cavity of the bolt will not guarantee a reliable installment. Hence, a sensor body is used, on which the SGs can be installed on the outside, enabling easy access for cleaning the application area, dosing the glue, applying pressure and check the installment, as was also used successfully by Groche et al. [19] or Herbst et al. [34]. The sensor body is then mounted inside a cavity of the bolt afterward using e.g. press fit, gluing or screwing-in, see Figures 2a, 2b, 4.

For a multi axial measurement, at least three SGs are to be installed on a sensor body with defined shape to be able to separate the measurement axes, see e.g. Figure 2b. When using Wheatstone bridge configurations to compensate disturbances and amplify the signal, the amount of SGs



(a)                                (b)
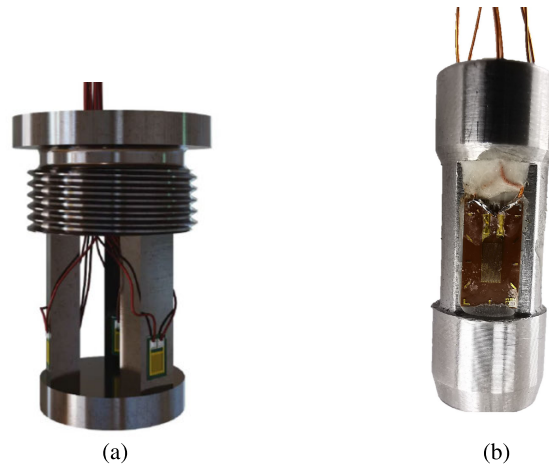
**FIGURE 2.** Sensor body examples for multi-axial force measurement. (a) Sensor body with strain gauges for screwing in and gluing from Herbst et al. [34], and (b) Sensor body with strain gauges for press fit.

needed increases by factor two: three half-bridges, see e.g. Figure 2a or factor four.

Furthermore, the electronics to read out the sensors and transmit the data as well as an energy storage for buffering needs to be housed inside the bolt to fulfill the requirements.

## C. DESIGN SPACE PARAMETERS, LOCATION AND SHAPE

Following the procedure introduced in Figure 1 step (2.1), with the knowledge from step (1), an initial design space is defined in shape and location. Then parameters are defined to be used in further calculations.

Therefore, analytical calculations are taken into account to estimate the stress distribution (indicator for the utilization of the material - loadability) of a bolt in a notched cross-section with regard to the load cases tensile force, bending and torsional torques. As geometry a cylindrical shape is considered resembling a bolt shaft close to the notch of the head, see Figure 3. Notches lead to an increase in stress especially at the edges. Therefore, the stress in the center decreases, since the overall stress in a cross-section must not change as shown in (1) [41]:

$$\int \sigma_n \, dA = F \tag{1}$$

where $\sigma_n$ is the normal stress and $A$ is the cross section area.

The unknown function of the stress with notch effect $\sigma_{z,notch}$ with respect to radius $r$ is calculated by using the second order approach:

$$\sigma_{z,notch}(r) = ar^2 + br + c. \tag{2}$$

The equation can be solved by symmetry boundary conditions, known boundary values at the edges, $\sigma_{z,notch}(r = R) = \alpha_z \sigma_n$, and

$$\int_R^R \sigma_n \, dr = \int_R^R \sigma_{z,notch}(r) \, dr. \tag{3}$$

This leads to tensile stress with notch effect (4):

$$\sigma_{z,notch}(r) = \frac{\sigma_{z,max}}{2}\left(\frac{3}{R^2}(\alpha_z - 1)r^2 + \frac{1}{2}(3 - \alpha_z)\right). \quad (4)$$

The bending stress with notch effect is calculated similarly (5):

$$\sigma_{b,notch}(r) = 3\frac{\sigma_{b,max}}{R^5}\left(\alpha_b - \frac{3}{2}\right)r^5$$
$$+ 2\frac{\sigma_{b,max}}{R^3}(2 - \alpha_b)r^3 + \frac{\sigma_{b,max}}{2R}r. \quad (5)$$

The torsional stress with notch effect is similar to the bending stress and calculated as follows (6):

$$\tau_{t,notch}(r) = |\ 3\frac{\tau_{t,max}}{R^5}\left(\alpha_t - \frac{3}{2}\right)r^5$$
$$+ 2\frac{\tau_{t,max}}{R^3}(2 - \alpha_t)r^3 + \frac{\tau_{t,max}}{2R}r\ |. \quad (6)$$

Since the focus is on the trend, (4)-(6) are normed to the maximum stress $\sigma_{i,max}, \tau_{t,max}$, meaning that the equations become independent of the loads $(F, M)$.

The maximum v. Mises stress for a 2D circular cross-section in the shaft's height of the bolt with respect to cavity diameter $d_1$ is calculated as shown in (7):

$$\sigma_{v,max}(d_1) = \sqrt{(\sigma_{z,max} + \sigma_{b,max})^2 + 3\tau_{t,max}^2} \quad (7)$$

Equation 8 shows the maximal tensile stress:

$$\sigma_{z,max}(d_1) = \frac{F_M + \text{KEF} \cdot F}{\frac{\pi(D-d_1)^2}{4}} \cdot \alpha_z \quad (8)$$

Equation 9 shows the maximal bending stress:

$$\sigma_{b,max}(d_1) = \frac{Fs}{\frac{\pi D^3}{32}} \cdot \frac{D^4}{D^4 - d_1^4} \cdot \alpha_b \quad (9)$$

Equation 10 shows the maximal torsional stress:

$$\tau_{t,max}(d_1) = \frac{M_G}{\frac{\pi D^3}{16}} \cdot \frac{D^4}{D^4 - d_1^4} \cdot \alpha_t \quad (10)$$

Equation 11 is the thread torque (from VDI 2230 [22]):

$$M_G = F_M \cdot \frac{d_f}{2}\left(\frac{P}{\pi d_f} + 1.155\mu_G\right) \quad (11)$$

The parameter values used for calculation are shown in Tables 1 and 2.

The results of (7) showing the stress distributions are in Section III-A. Based on them, a cylindrical shape aligned in the center is chosen because it is the most reasonable shape according to the stress distribution with forces from unknown directions. Thus, the parameters of the design space are defined as shown in Figure 3. Parameters $d_1$ and $h_1$ form the sensor cavity, $d_2$ and $h_2$ the electronics cavity.

Parameters $d_1$ and $d_2$ are varied in the scope of this contribution, because the diameters have a high influence on the stress as can be seen in (8)-(10). Parameters $h_1$ and $h_2$ are set to fixed values. As long as $h_2$ is not protruding in the area of the thread, its influence is insignificant (see Appendix). The parameter values for this contribution are shown in Table 2.

**TABLE 1.** Parameters and values for analytical v. Mises stress calculations.

| parameter name | symbol | value |
|---|---|---|
| radius | $r$ | [0..10] mm |
| maximum radius R for M20 [21] | $R$ | 10 mm |
| pretension force | $F_M$ | 40 kN |
| operational force | $F$ | 40 kN |
| load introduction factor [22] | KEF | 0.05 |
| eccentricity of operational force | $s$ | 32 mm |
| outer diameter of M20 bolt [21] | $D$ | 20 mm |
| stress concentration factor tensile [42] | $\alpha_z$ | 2.49 |
| stress concentration factor bending [42] | $\alpha_b$ | 2.23 |
| stress concentration factor torsion [42] | $\tau_t$ | 1.63 |
| thread flank diameter M20 bolt [42] | $d_f$ | 18.327 |
| thread pitch M20 [21] | $P$ | 2.5 mm |
| thread friction [22] | $\mu_G$ | 0.2 |
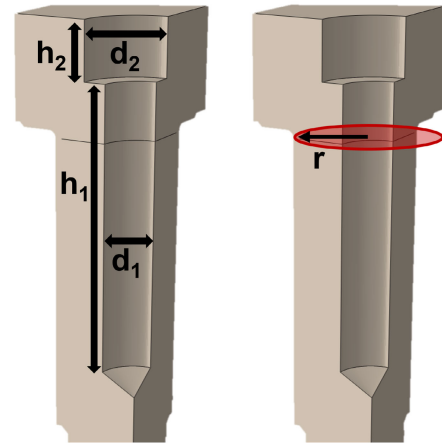


**FIGURE 3.** Design space parameters, $d_1$, $d_2$ are varied, heights are fixed (left). Cross-section in notch head/shaft (red) used to calculate the stress distribution with respect to radius $r$ (right).

**TABLE 2.** Design space parameters with value ranges used for further calculations.

| parameter name | symbol | value |
|---|---|---|
| diameter of sensor cavity | $d_1$ | [0..14] mm |
| height of sensor cavity | $h_1$ | 32 mm |
| diameter of electronics cavity | $d_2$ | [0..18] mm |
| diameter of sensor cavity | $h_2$ | 6.5 mm |

## D. FE MODEL AS BASE FOR MECHANICAL AND SENSORY FUNCTION MODELLING

According to the procedure introduced in Figure 1 step (4) a FE model is set up to retrieve outputs for modelling the mechanical and sensory function. Therefore, v. Mises stresses and strains are used.

The FE analysis is conducted with Abaqus 2022 (Simulia, Dassault Systèmes, Vélizy-Villacoublay, France). Both geometry modelling and meshing is done by using Abaqus' built-in tools. The geometry is modelled as a bolt tensioned between two blocks (Figure 5), which resembles the physical test rig that is used for verification of the model (Figure 10). The design space parameters $d_1, d_2, h_1, h_2$ are shown in Table 2 and Figure 3. Various parameter combinations are simulated, shown as white dots in the results, see
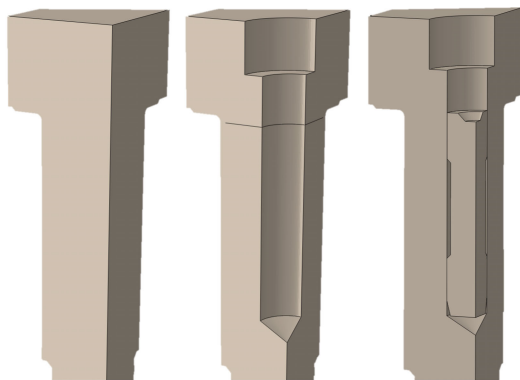
**FIGURE 4.** Example of design space parameter sets that are simulated in the FE analysis; Solid bolt (left), cavities (middle), press-fitted sensor body (right).

**TABLE 3.** Number of elements of the mesh.

| part name | elements total | C3D8R | C3D8 | C3D10 |
|---|---|---|---|---|
| Bolt | 168873 | 163653 | 5220 | - |
| Upper block | 49125 | 3888 | 2730 | 42507 |
| Lower block | 45006 | 7360 | - | 37760 |

Figures 14 and 16. The solid bolt with no cavities ($d_1 = 0$ mm, $d_2 = 0$ mm) serves as reference for the stress increase.

Results are retrieved for models with and without a press-fitted sensor body, see Figure 4. The press fit is achieved by use of a cylindrical interference press fit H7s6 (tolerances: bore $d_1$ $\varnothing 10_0^{+15}$ mm, sensor body: $\varnothing 10_{+23}^{+32}$ mm). These versions serve the purpose to investigate the effect of the sensor body on the FE outputs.

The FE model is shown in Figure 5, the elements in Table 3. Hexahedral elements with reduced integration (C3D8R) are used to mesh the bolt and all the sections near contact surfaces. Additionally, the hexahedral elements in the contact surfaces are without reduced integration (C3D8) to reduce penetration of the elements. Critical sections like the notches of the bolt have a finer mesh density to give more accurate results. The parts are partitioned to allow meshing of the more complex geometries and separate the areas with finer and coarser meshes. Tetrahedral elements (C3D10) are used for the sections of the blocks that are not in contact with another part.

One of the most critical surface interactions in the system is between the bolt's and the lower block's threads. This is modelled with the smear contact interaction [43], implemented as a special function from Abaqus.

The load is 40 kN pretension force and 40 kN tensile operational force. Tensile forces have the most effect on the v. Mises stress increase for cavities in the shaft, as section III-A shows. The forces are below the maximum force that the material class of the modelled bolt can bear to stay in the linear elastic area. To reduce calculation time, only a quarter of the bolt is modelled for tensile load cases. The material for the model is chosen to be of bolt strength class 8.8, which has a yield strength of 640 N/mm$^2$.
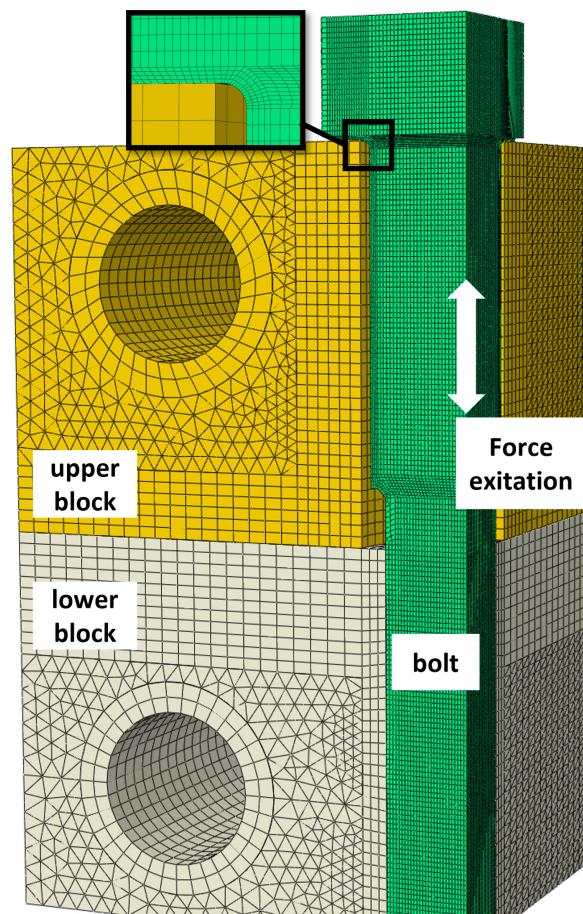


**FIGURE 5.** Meshed FE model of bolt as a quarter model, version without cavity.

### E. MODELLING THE MECHANICAL FUNCTION

The next step in the procedure shown in Figure 1 is step (5.1), modelling the mechanical function. The mechanical function of a standard metrical bolt is to apply clamping force between its head and thread. This results in a load (force or torque) acting on the bolt which leads to stresses in the bolt's material, as shown in Figure 11.

The v. Mises stress is used to evaluate the mechanical function, as is established in the state of the art and also used successfully by Bonaiti et al. [35] or Dumstorff et al. [25].

The basic concept of modelling the v. Mises stress to the design space parameters is shown in Figure 6. The output is the normed change of the maximum v. Mises stress, resembling a mechanical function fulfillment index (MFI), with respect to the design space parameters $d_1$, $d_2$. The inputs are the aforementioned design space parameters and the load (force, lever) conditions. A FE model (see section II-D) provides the v. Mises stresses as interim result. The stress data points are curve fitted to retrieve a function of stress with respect to the design space parameters. The curve fitting is done with MATLAB 2022b (MathWorks, MA, USA). Afterward, the function is normalized to the maximum v. Mises stress of the bolt without cavities ($d_1 = d_2 = 0$), which
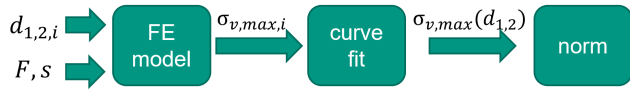
**FIGURE 6.** Model which outputs mechanical function fulfillment index (MFI) with respect to design space parameters $d_1$, $d_2$; a FE model calculates the maximum v. Mises stresses $\sigma_{v,max}$ depending on $d_1$, $d_2$ and load case $F$, $s$, the $i$ indicating variation data sets of $d_1$, $d_2$.



**FIGURE 7.** Model which outputs sensory function fulfillment index (SFI) with respect to design space parameters $d_1$, $d_2$; a FE model calculates the strain at the sensor position at the shaft $\varepsilon_{shaft}$ depending on $d_1$, $d_2$ and load case $F$, $s$, the $i$ indicating variation data sets of $d_1$, $d_2$.

is defined as mechanical function fulfillment index (MFI), shown in (12):

$$\text{MFI} := \sigma_{v,norm}(d_1, d_2) = \frac{\sigma_{v,max}(d_1, d_2)}{\sigma_{v,max}(0, 0)}. \qquad (12)$$

### F. VERIFYING THE FE STRESS OUTPUT FOR THE MECHANICAL FUNCTION

To verify the FE model output and the normalization (step 5.4), the normalized global maximum of the v. Mises stress is compared to the analytical equation results at cross-section of the notch head/shaft as shown in (13):

$$\sigma_{v,norm}(d) = \frac{\sigma_{v,max}(d)}{\sigma_{v,max}(0)}. \qquad (13)$$

The cavity diameters are varied accordingly, with $d_1 = d_2 = d$ to ensure a good comparability with the analytical calculation (7), which is only formulated for one diameter.
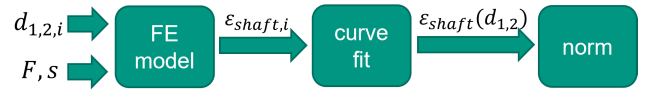
### G. MODELLING THE SENSORY FUNCTION

For modelling the sensory function (step 5.5 and following) the theoretically achievable measurement quality with focus on the sensor part is considered, depending on the design space parameters (see section II-C). Therefore, the physical strain subjected to the strain gauges is analyzed. With more strain there is a higher achievable signal-to-noise ratio because the measuring range can be exploited more, as shown in the following basic formulas of strain gauges linking the strain to the measurand, see (14) and [44], [45]. In the scope of this contribution this is the only influence regarded on the sensory function fulfillment.

$$\varepsilon k = \frac{\Delta R}{R} \qquad (14)$$

$\varepsilon$ is the physical strain subjected on the gauge, $k$ is the strain gauge's sensitivity or gauge factor (data sheet value), $\Delta R$ is the strain gauge's change of resistance due to strain and $R$ is nominal resistance of the undeformed gauge. This shows that for higher strains there is a higher measurand which can be sampled with a higher signal-to-noise ratio, leading to a more accurate force prediction. Hence, the sensory function fulfillment index (SFI) is dependent on the strain as follows (15):

$$\text{SFI}(d_{1,2}) \propto \varepsilon(d_1, d_2) = \frac{\Delta R(d_1, d_2)}{Rk} \qquad (15)$$

For this function the strain at the middle of the bolt's shaft is considered, which is the most likely position for strain gauges, see II-B).

The concept of the sensory model is shown in Figure 7. The output is a sensory function fulfillment index, composed of the subjected physical strain on the strain gauges position with varying cavities (design space parameters). The inputs are the aforementioned design space parameters $d_1$, $d_2$ and the load (force, torque) conditions. The FE-model will provide the strain outputs as an interim result. The data points are curve fitted to a function of strain with respect to the design space parameters. Afterward the function is normalized, divided by the strain at the strain gauges position for $d_1 = d_2 = 0$ mm, which is defined as SFI see (16):

$$\text{SFI} := \varepsilon_{shaft,norm}(d_1, d_2) = \frac{\varepsilon_{shaft,norm}(d_1, d_2)}{\varepsilon_{v,norm}(0, 0)}. \qquad (16)$$

Furthermore, the SFI which is based on the strain is linked to the target quantity of the sensory function, which is force measurement. Strain gauges are usually measured within a Wheatstone bridge to compensate for disturbances and amplify the signal, where the change of resistance results in a change of voltage. Using (17) and 18 from [44] and [45], the axial force $F_n$ is linked to the output voltage of the Wheatstone bridge. The equations are only valid for linear elastic behavior of the materials and for a quarter bridge configuration.

$$F_n = A\sigma_n = AE\varepsilon_n \Rightarrow F_n \propto \varepsilon_n \qquad (17)$$

$$\varepsilon = \frac{4}{k}\frac{V_o}{V_s} \qquad (18)$$

$A$ is the minimal cross-section area considering the force flow, $\sigma_n$ is the normal stress, $\varepsilon_n$ the normal strain, $E$ is the Young's modulus, $V_o$ is the output voltage of the Wheatstone bridge, $V_s$ is the supply voltage of the Wheatstone bridge.

Finally, with knowledge of the measurement chain, the resolution of the force can be derived by taking the effective number of bits (ENOB) into account, defined by the resolution, gain and noise of the analog-digital converter (ADC). In order to get the lowest measurable force, $V_o$ in (18) is replaced by $V_{ref}/(2^{\text{ENOB}})$, with $V_{ref}$ being the reference voltage of the ADC (depending on the setup $V_{ref}$ can be the same as $V_s$), see (19)-(21).

$$\varepsilon_{min} = \frac{4}{k}\frac{V_{ref}}{V_s 2^{\text{ENOB}}} = \frac{4}{k}\frac{1}{2^{\text{ENOB}}} \qquad (19)$$

$$F_{n,min} = AE\varepsilon_{n,min} = AE\frac{4}{k}\frac{V_{ref}}{V_s 2^{\text{ENOB}}} = AE\frac{4}{k}\frac{1}{2^{\text{ENOB}}} \qquad (20)$$

$$\text{ENOB} = \log_2\left(\frac{4}{k}\frac{1}{\varepsilon_{min}}\right) = \log_2\left(\frac{4}{k}\frac{AE}{F_{min}}\right) \qquad (21)$$

**FIGURE 8.** Node in the FE-model for strain evaluation (left) and applied strain gauges on the bolt with cavities $d_1 = 10$ mm and $d_2 = 13$ mm on the outside of the shaft, 3 strain gauges are spaced symmetrically in the cross-section (right).



**FIGURE 9.** Node in the FE-model for strain evaluation (left) and cylindrical strain gauge applied in bolt with single cavity $d_1 = d_2 = 2$ mm (right).

## H. VERIFYING THE FE STRAIN OUTPUT FOR SENSORY FUNCTION MODELLING

Following the procedure from Figure 1 step 5.8 the strain output of the FE model at specified nodes is compared to strain gauge measurements in a universal testing machine (model 112.50kN, TesT, Erkrath, Germany) (see Figure 10). Therefore, strain measurements of three strain gauges that are applied on the outside of the bolt shaft (Type: 1-LY41-3/350, HBM, Darmstadt, Germany), see Figure 8, and one cylindrical strain gauge in a small drill hole of 2 mm (Type: 1-LB11-3/120ZW, HBM, Darmstadt, Germany), see Figure 9, are compared to the FEM-model's strain output at a point resembling the strain gauge's position. The amplifier GSV-1A4 (ME-Systeme, Hennigsdorf, Germany) is used, which has a reference voltage of 5 V and a sensitivity of 2 mV/V and a range of $+/- 10$ V. The offset was compensated before every test run.

## I. COMBINING MODELS TO OPTIMIZATION FUNCTION

The mechanical and sensory part of the function fulfillment are combined within one function (symbol $O$) with respect to the design space parameters. In order to achieve adaptability
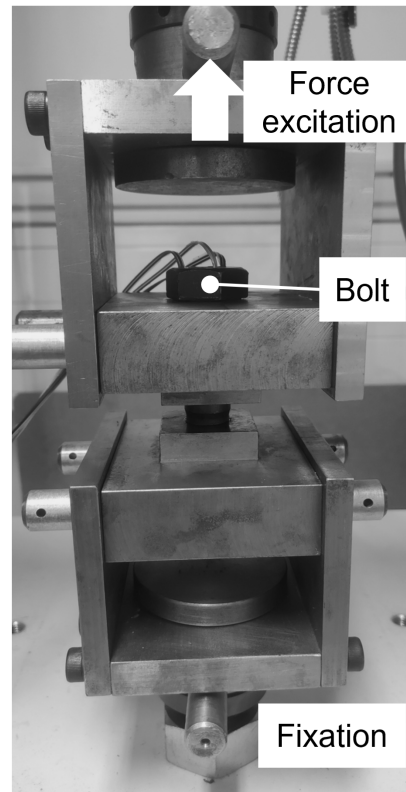


**FIGURE 10.** Test rig used for verification, bolt with applied strain gauges in universal test machine for evaluation of strain gauge measurements to compare with FE model output.

of the sensory and mechanical function fulfillment index, the subcomponents are given weighting factors $w_{mech}, w_{sens}$ and are used as the exponent of an exponential function. With these, prioritizing the mechanical versus the sensory part is possible. The subcomponents $\sigma_{v,max}, \varepsilon_{shaft}$ are normed to achieve better aligning and have more feasible weights, as shown by Sahib et al. [46]. The part for $\varepsilon_{shaft}$ is inverted to get an opposing behaviour to the monotonously rising $\sigma_{v,max}$. The mechanical and sensory part are multiplied, as shown in (22).

$$O(d_1, d_2) := exp\left(w_{mech}\frac{\sigma_{v,max}(d_1, d_2)}{\sigma_{v,max}(0, 0)}\right)$$
$$\cdot exp\left(w_{sens}\frac{\varepsilon_{shaft}(0, 0)}{\varepsilon_{shaft}(d_1, d_2)}\right) \quad (22)$$

For the weights the following definition is used:

$$w_{mech} = 1 - w_{sens}, w_{mech} = [0..1] \quad (23)$$

To solve the optimization function for minima, MATLAB's optimization toolbox is used with standard solver "fmincon" with interior-point setting. Diameters $d_1, d_2 \geq 0$ are used as boundary condition next to (25).

## III. RESULTS

First, the initial design space parameter considerations will be shown. Then, the modelling for the mechanical and sensory
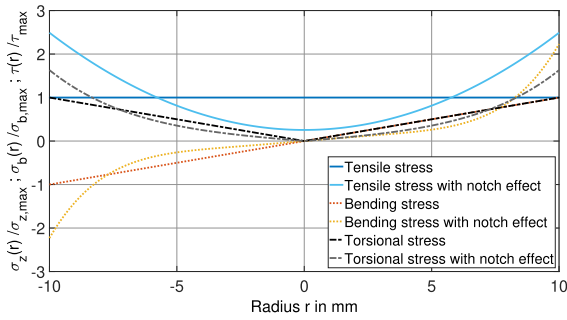
**FIGURE 11.** Comparison of normed trends of tension for tensile, bending and torsional load cases in cross-section notch head/shaft of a M20 bolt with and without consideration of notch effect; with notch effect the stress increases on the outside ($r = +/- 10\,mm$) and decrease on the inside of the bolt's cross-section, compared to the case without notch effect consideration; for tensile load case with notch effect the stress has the highest increase at the outside ($r = +/- 10\,mm$).

part will be presented separately together with the function that is retrieved. Then, the functions will be merged together to a single optimization function.

### A. INITIAL DESIGN SPACE CONSIDERATIONS - LOCATION AND SHAPE

Based on the analytically calculated stress distributions, a reasonable location and shape for the cavity is identified. Figure 11 shows the stress distribution with respect to the radius of a cross-section in the shaft with an outer diameter ($D$) of 20 mm and a cavity diameter ($d_1$) of 0 mm for three load cases. For bending and torsional loads, without consideration of any notch effects, the stress at the outside is higher than on the inside of the bolt (blue line in plots). When considering the effect of the notch head/shaft, this effect is amplified and even appears on the tensile load case (orange line in plot). Notches shift the stress to the outer edges.

This leads to the conclusion, that cavities in the center of the bolt are best suited to prevent substantial losses in the mechanical function. Because the load direction, especially for bending loads, is unknown, cylindrical cavity shapes are the best option.

It also shows that considering the tensile load case for stress increase is the most reasonable, because the factor is 2.5, which is slightly more compared to the bending case (2.2) and much more compared to the torsional case (1.6). Due to this, it is chosen as the most critical load case for the FE analysis in the next section.

### B. MECHANICAL FUNCTION MODEL

The first step of the mechanical model is the relation from the design space parameters (diameters) to the v. Mises stress.

Figure 12 shows exemplary the v. Mises stress $\sigma_v$ distribution in the bolt with cavity diameters $d_1 = 10\,mm$ and $d_2 = 13\,mm$ at a pretension load of 40 kN and a tensile operation force of 40 kN. The highest stress is in the notch head/shaft of the bolt for all versions simulated.
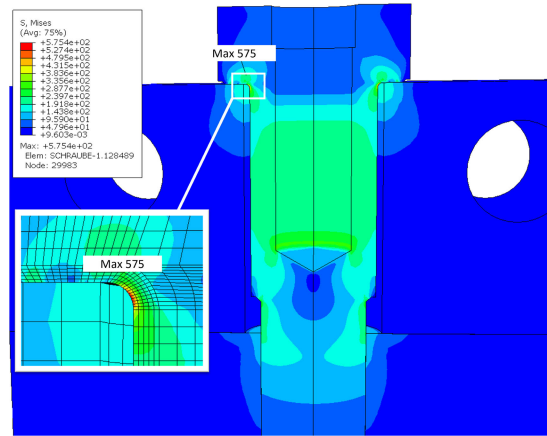


**FIGURE 12.** V. Mises stress of the bolt with cavity diameters $d_1 = 12\,mm$ and $d_2 = 13\,mm$, maximum of 575 N/mm$^2$.
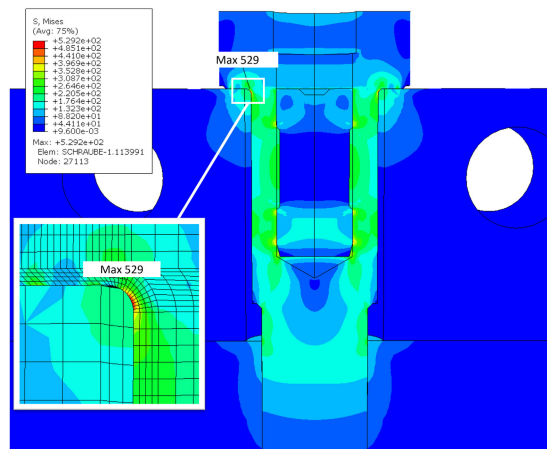


**FIGURE 13.** V. Mises stress of the bolt with press fitted sensor body and cavity diameters $d_1 = 12\,mm$ and $d_2 = 13\,mm$, maximum of 529 N/mm$^2$.

The press-fitted sensor body is able to reduce the stress in the bolt, especially the maximum stress in the notch head/shaft, see Figure 13.

The design space parameter combinations that were simulated in the FE analysis are shown in 14 as black points. A fit on the stress outputs for those parameter combinations as a matrix was performed with MATLAB using third order polynomials in the $d_1$ and the $d_2$ directions respectively. As fit method Linear Least Squares was chosen with bisquare robust settings that minimize the summed square of the residuals, and reduce the weight of outliers using bisquare weights. As fitting algorithm Trust-Region was chosen. The coefficient $p_{00}$ can be regarded as the constant offset of the function and therefore was constrained to be between 460 N/mm$^2$ and 480 N/mm$^2$, which is the value for the bolt without cavities (see Figure 14, 469 N/mm$^2$ for $d_1 = d_2 = 0$). Equation 24 shows the function with respect to $d_1$ and $d_2$, spanning a surface. Figure 14 shows the resulting surface. The $R^2$ of the fit is 0.988. The values of the polynomials from the
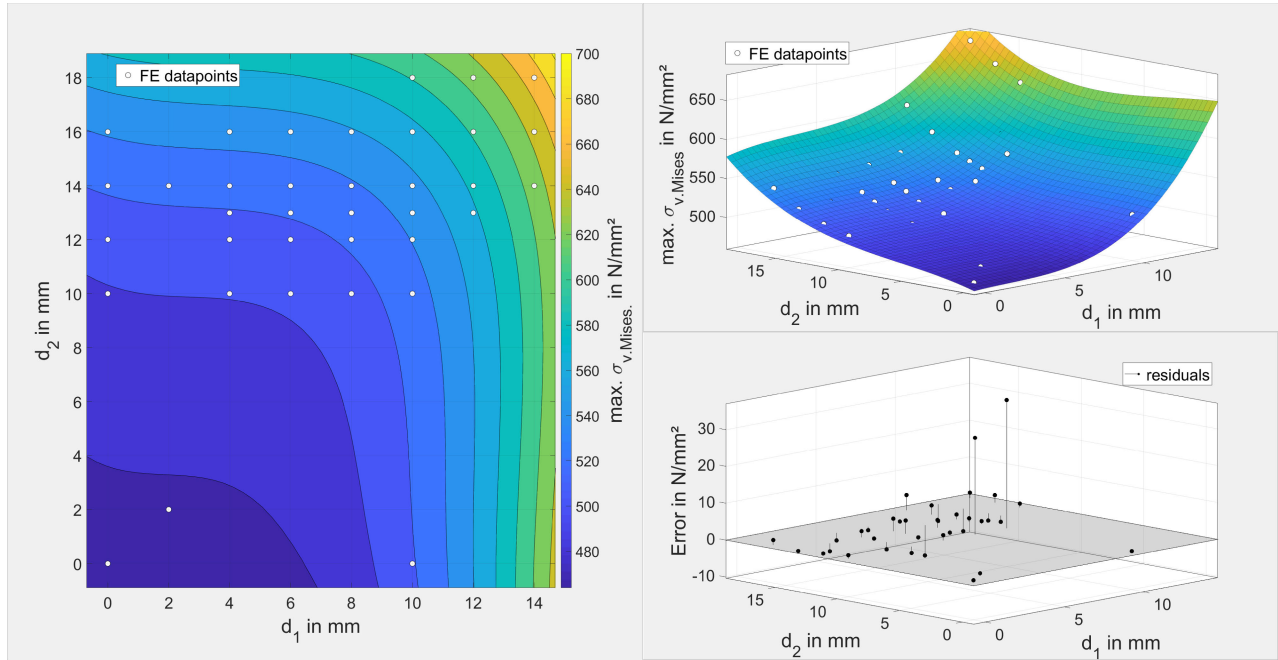
**FIGURE 14.** V. Mises stress and fit for tensile load case with respect to $d_1$ and $d_2$, FE model output shown as black points, showing increase of stress with rising $d_1$ or $d_2$; residuals plot shows the error of the fitted surface to the FE model data points.

**TABLE 4.** Coefficients $p_{ij}$ for fitted surface of v. Mises stress with respect to $d_1$ and $d_2$.

| | | | |
|---|---|---|---|
| $p_{00}$ | $468.6 \, \text{N/mm}^2$ | $p_{02}$ | $-0.344 \, \text{N/mm}^4$ |
| $p_{10}$ | $0.8555 \, \text{N/mm}^3$ | $p_{30}$ | $0.07579 \, \text{N/mm}^5$ |
| $p_{01}$ | $4.098 \, \text{N/mm}^3$ | $p_{21}$ | $-0.02594 \, \text{N/mm}^5$ |
| $p_{20}$ | $-0.3474 \, \text{N/mm}^4$ | $p_{12}$ | $0.009642 \, \text{N/mm}^5$ |
| $p_{11}$ | $-0.001394 \, \text{N/mm}^4$ | $p_{03}$ | $0.02339 \, \text{N/mm}^5$ |

fit are shown in Table 4.

$$\sigma_{v,fit}(d_1, d_2)$$
$$= p_{00} + p_{10}d_1 + p_{01}d_2 + p_{20}d_1^2 + p_{11}d_1d_2$$
$$+ p_{02}d_2^2 + p_{30}d_1^3 + p_{21}d_1^2d_2 + p_{12}d_1d_2^2 + p_{03}d_2^3 \quad (24)$$

Ensuring the mounting of the sensor body, $d_2$ needs to be equal or greater than $d_1$, resulting in the following boundary condition (25):

$$d_2 \geq d_1. \quad (25)$$

Following the procedure introduced in section II-E the fitted function is now normed to the v. Mises stress of the bolt without cavities, Figure 20.

## C. VERIFICATION OF FE OUTPUT STRESS

Figure 15 shows the normed v. Mises stress output of the FE model as well as the analytical equation of the v. Mises stress (7). For cavity diameters $d_1 \leq 10$ mm there is a good match. However, for bigger diameters the analytic calculation gives back higher stress increases than the FE-model.
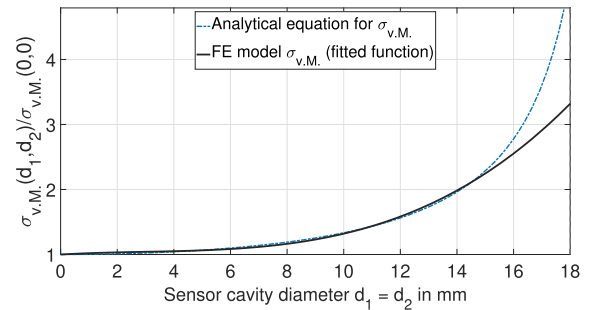


**FIGURE 15.** Normed v. Mises stress for tensile load case, comparison between FE model output and analytic equations; good match for $d_1 < 16$ mm proving usability of the FE model outputs.

## D. SENSORY FUNCTION MODEL

For the sensor function fulfillment index $SFI(d_1, d_2)$ concerning measuring range exploitation, the strain data of the shaft from section III-B are taken, originating from the FE model outputs.

Following the same procedure used in the mechanical modelling, a fit on those data points using MATLAB was performed with third order polynomials in the $d_1$ and the $d_2$ directions respectively. The approach and curve fitting method is the same as used for the mechanical part, only with $\varepsilon$, see (26). Figure 16 shows the resulting surface. The $R^2$ of the fit is 0.98. The values of the polynomials from the fit are shown in Table 5.

$$\varepsilon_{shaft,fit}(d_1, d_2)$$
$$= p_{00} + p_{10}d_1 + p_{01}d_2 + p_{20}d_1^2 + p_{11}d_1d_2$$
$$+ p_{02}d_2^2 + p_{30}d_1^3 + p_{21}d_1^2d_2 + p_{12}d_1d_2^2 + p_{03}d_2^3 \quad (26)$$
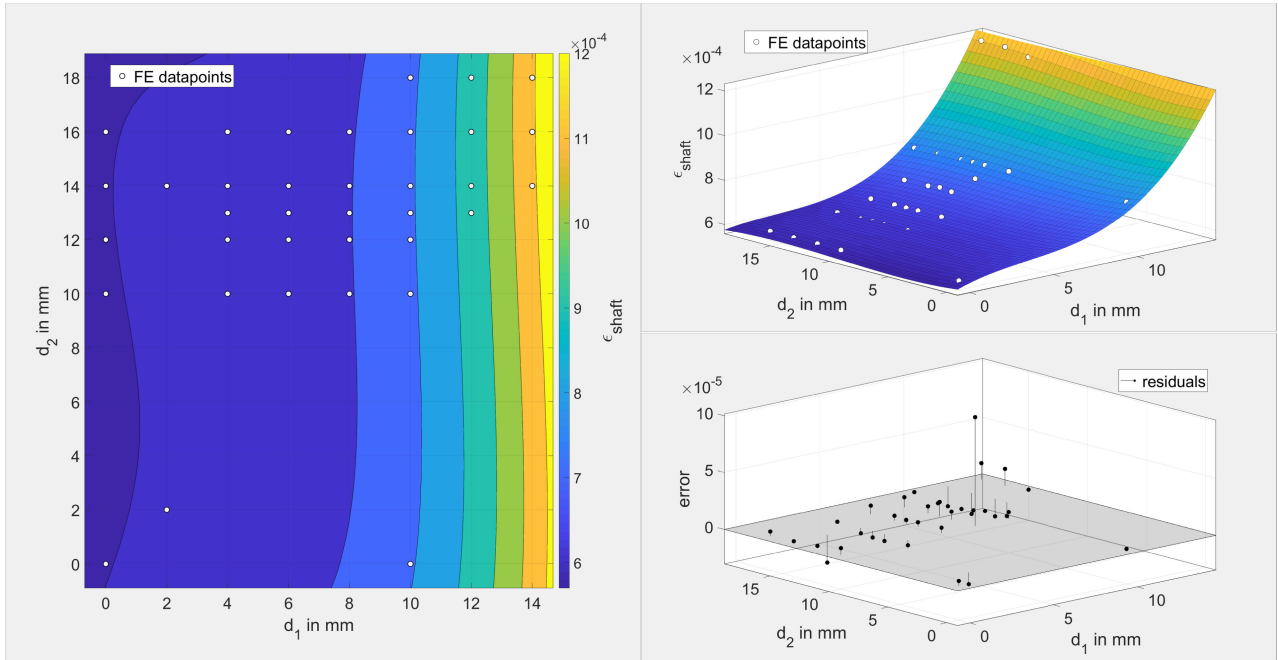
**FIGURE 16.** Strain at shaft and fit for tensile load case with respect to $d_1$ and $d_2$, FE model output shown as white dots, showing increase of strain with rising $d_1$, $d_2$ has very low influence; residuals plot shows the error of the fitted surface to the FE model data points.

**TABLE 5.** Coefficients $p_{ij}$ for fitted surface of strain at shaft with respect to $d_1$ and $d_2$.

| | | | |
|---|---|---|---|
| $p_{00}$ | $5.95 \cdot 10^{-4}$ | $p_{02}$ | $8.276 \cdot 10^{-7}$ 1/mm$^2$ |
| $p_{10}$ | $2.055 \cdot 10^{-5}$ 1/mm | $p_{30}$ | $3.472 \cdot 10^{-7}$ 1/mm$^3$ |
| $p_{01}$ | $-5.537 \cdot 10^{-6}$ 1/mm | $p_{21}$ | $5.787 \cdot 10^{-8}$ 1/mm$^3$ |
| $p_{20}$ | $-3.562 \cdot 10^{-6}$ 1/mm$^2$ | $p_{12}$ | $2.876 \cdot 10^{-9}$ 1/mm$^3$ |
| $p_{11}$ | $-6.418 \cdot 10^{-7}$ 1/mm$^2$ | $p_{03}$ | $-3.005 \cdot 10^{-8}$ 1/mm$^3$ |

Following the procedure introduced in section II-G the fitted function $\varepsilon_{shaft,fit}$ is now normed to the function's value at $d_1 = d_2 = 0$ mm. The resulting sensory function fulfillment index SFI is shown in the contour plot of Figure 21. The best fulfillment scores are at high diameters $d_1$. However, $d_2$ hardly has an effect on the SFI. For usage of this part in the optimization function, the SFI is inverted to have best scores at with low values.

### E. VERIFICATION OF FE OUTPUT STRAIN

Figure 17 shows the strain output of the FE model and the three strain gauges (SG) at varying loads for comparison. The strain of the SGs follow the slope of the FE output, but deviate slightly from it and also deviate from each other. The relative error for two of the SGs reduces from 30% to 20%, the error of the third is relatively steady at around 1%.

Figure 18 shows the strain output of the FE model and the cylindrical SG at varying loads for comparison. The strain of the SG follows the slope of the FE output very accurate, only deviating slightly from it at the end by growing closer to the FE model output, reducing the relative error to below 10%.
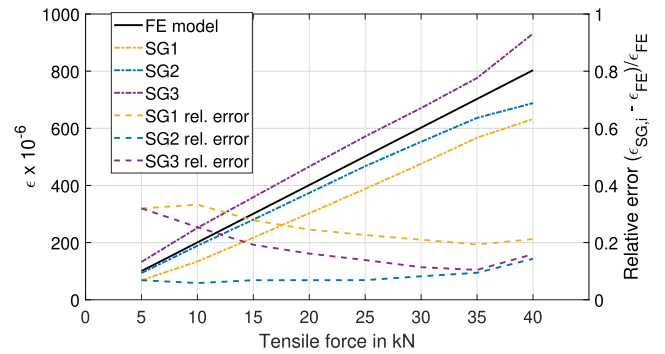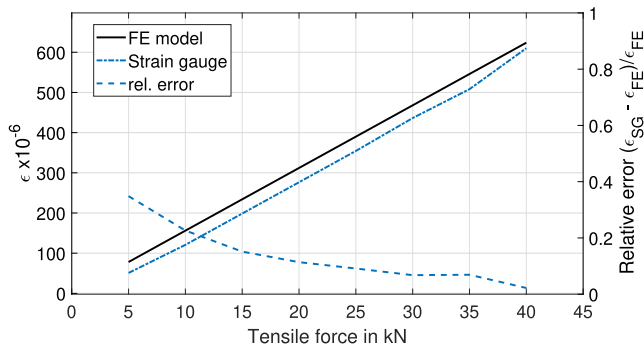


**FIGURE 17.** Comparison of FE model and three strain gauge measurements on bolt's shaft with cavities $d_1 = 10$ mm and $d_2 = 13$ mm; the slopes of the strain gauge measurements follow the FE model output. There is a relative error of 30% which decreases for higher loads to 20% and below.

### F. COMBINED MODELS TO ESTIMATE OPTIMAL DESIGN SPACE PARAMETERS

According to section II-A the mechanical and sensory part of the function fulfillment are combined within one optimization function (symbol $O$), to get optimal design space parameters $d_1$, $d_2$.

Figure 19 shows a series of contour plots of the optimization function with varying weights according to (23). As to be expected, the highest fulfillment scores (the minima in dark blue) shift with the weighting: high $w_{mech}$ and low $w_{sens}$ result in best scores at low $d_1$, $d_2$ and vice versa.

For equal weights of mechanical and sensory part (both 0.5 in Figure 19), the best scores are at $d_1 = 13.7$ mm and $d_2 = 9$ mm, however not satisfying boundary condition (25),

**FIGURE 18.** Comparison of FE model and strain gauge measurements on bolt with cylindrical strain gauge (SG) in cavities $d_1 = 2$ mm and $d_2 = 2$ mm); the strain of the SG follows the slope of the FE output very close, the relative error is below 0.1 for loads higher than 25 kN.

$d_2 \geq d_1$. With respect to the boundary condition the values $d_1 = d_2 = 13.2$ mm are the optimum, with $MFI = 1.29$, $SFI = 1.81$. This shows that the effect of the parameters on the sensory function is higher than on the mechanical function. This can also be seen when comparing Figure 20 to 21 : the effect of the cavity diameters on the strain at the shaft (sensory function) is higher than their effect on the maximum stress (mechanical function).

## IV. DISCUSSION

This chapter contains example use cases, comparisons with the state of the art, limitations of the results, summary and outlook.

### A. EXAMPLE USAGE OF THE OPTIMIZATION FUNCTION AND INTERIM RESULTS

There are several ways to use the functions modelled in this contribution, depending on the requirements:

1) mechanical requirements first,
2) sensory requirements first,
3) both mechanical and sensory requirements simultaneously.

A **mechanical requirement** to start with is a definition of a maximum stress increase. This application specific and can usually be extracted out of a thorough analysis. For this purpose we define a maximum stress increase of 25%, factor 1.25 (from 469 N/mm$^2$ to 582 N/mm$^2$ for load case in this contribution), because this is in a range that can be compensated by increasing the material strength class by one level. Formulated as a condition we get (27):

$$\text{MFI}(d_1, d_2) \leq 1.25. \tag{27}$$

Possible solutions for $d_1, d_2$ fulfilling this condition are outlined in Figure 20 by the red dotted line. To fix values for the parameters, one needs to be defined, or further boundary conditions need to be specified. In this example we choose electronics cavity diameter to be $d_2 = 14$ mm. At the intersection of $d_2$ and (27) contour line the missing parameter $d_1 \approx 12$ mm is found.

For this set of design space parameters, the sensory function fulfillment index can be calculated with (24) for $\varepsilon$ and coefficients from Table 5 or read from Figure 21. In this case: $SFI \approx 1.59$, hence the strain at the shaft increases by $= 59\%$ which corresponds to a strain of $\varepsilon = 9.47 \cdot 10^{-4}$ for the load case used in this work. Using (18) the measurement output of the Wheatstone bridge can be calculated, which is $V_o/V_s = 485\,\mu$V/V. Following (19), the ADC needs an ENOB of 11 bits. In order to measure a change of 1% of the load (in this case 800 N), the ENOB increases to 18 bits. Using these models engineers are enabled to decide if the measurement chain is feasible, or if an iteration is needed by lowering the MFI, for example.

In the case of **sensory requirements** only, the procedure is similar to the above-mentioned, only switching the steps: checking the sensory requirement is done first by solving the $SFI$ equation or graphically in the contour plot, Figure 21. The boundary condition chosen for $SFI$ is shown in (28) a solution fulfilling this condition is shown in Figure 21.

$$\text{SFI}(d_1, d_2) \geq 2.9 \tag{28}$$

The MFI for this case is 1.62, hence the v. Mises stress increases by 62% compared to the bolt without cavities. This means that the bolt strength class needs to be increased of about three classes (each class has an increase in yield strength of about 20%). For the load case investigated in this contribution the v. Mises stress increases from 469 N/mm$^2$ to 760 N/mm$^2$. With this value a bolt strength class of 10.9 can be chosen.

In the case of **requirements from both mechanical and sensory side**, they need to be prioritized initially by adjusting weights for the optimization function. In this case, we use weights $w_{mech} = w_{sens} = 0.5$. Further, boundary conditions for mechanical and sensory functions are defined to get a solution that fits to a usage scenario, see (29) and (30).

$$\text{MFI}(d_1, d_2) \leq 1.1 \tag{29}$$
$$\text{SFI}(d_1, d_2) \geq 1.2 \tag{30}$$

The optimization function together with the boundary conditions is implemented into the solver, which returns an optimal DS parameter set of $d_1 = d_2 = 8.8$ mm. $MFI$ is 1.1 as requested which means an increase of v. Mises stress by 10%, $SFI$ is 1.22 which means an increase of strain at the sensor position of 22%.

### B. COMPARISON WITH THE STATE-OF-THE-ART

The sensor concept for a sensor body and cavity inside a bolt published in prior work by Herbst et al. [34] served as an example case. The results are similar for the v. Mises stress increase at the cavity parameters. The authors presented stress increases of one material strength class from 5.6, which are about 20% to 25%, for a sensor cavity diameter of 12 mm. The results of this paper also show an increase of 25% for a sensor cavity of 12 mm in the shaft and 14 mm in the head. This suggests that the FE-modelling is comparable and underlines its validity.
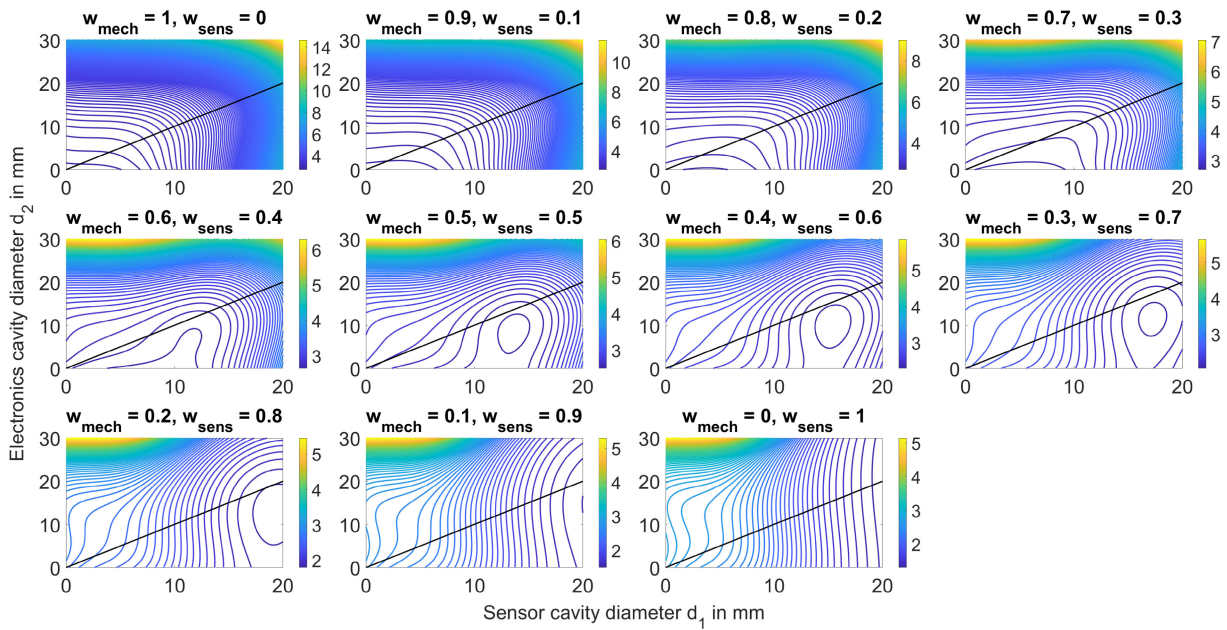
**FIGURE 19.** Combined optimization function for varying weights, the best fulfillment scores are the minima shown in dark blue; black line shows $d_1 = d_2$, only combinations above this line are reasonable considering mountability of sensors.
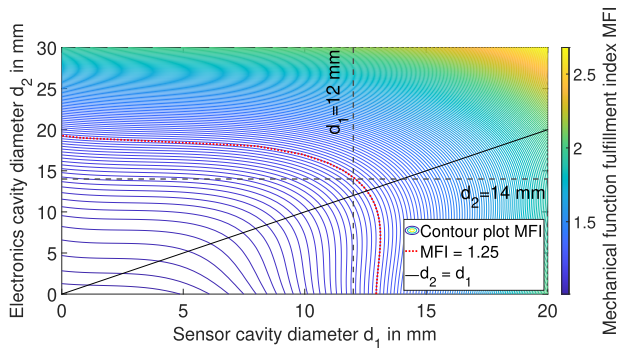


**FIGURE 20.** Mechanical function fulfillment index for $d_1$, $d_2$ with condition of minimum $MFI \leq 1.25$ and assumed $d_2 = 14$ mm, resulting in $d_1 = 12$ mm.
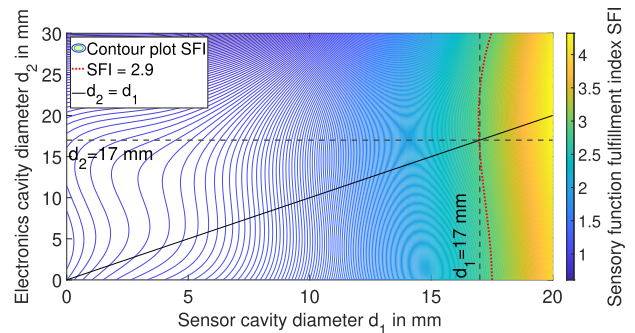


**FIGURE 21.** Sensory function fulfillment index for $d_1$, $d_2$ with condition of $SFI \geq 2.9$; $d_2$ is set to its minimum following the boundary condition $d_2 \geq d_1$; solution at the boundary condition in this case is $d_1 = d_2 = 17$ mm.

Another example case for a sensor concept regarded in the scope of this contribution was proposed by Groche et al. [19]. Stress or strain were not provided by the authors, only the relative stiffness. When analyzed in a relative manner, the force, Young's modulus and length are cancelled out and the stiffness can be compared to the strain in a relative manner. Given the cavity dimensions from Groche et al. of 45% of the outer diameter the stiffness changes 26% relative to the full body. This is close to the change of strain of 23% for a 45% cavity diameter from this contribution (Figure 21 values at $d_1 = d_2 = 0$ mm and $d_1 = d_2 = 9$ mm). Furthermore, the statement that stiffness is linked to the sensitivity of the sensors can be supported. The formulas from strain gauges linking the strain to the change in resistance used in this contribution show an increase in measuring range to be exploited. Further, the results from Groche et al. suggest

that the sensor body fitted into the bolt structure is able to reduce some of the effects of the cavity. This can also be seen in the comparison of the FE model outputs between the hollow cavity and the press fitted sensor body. For example, comparing the stress of the bolt with cavity diameters $d_1 = 10$ mm and $d_2 = 13$ mm (see Figures 12, 13) there is a stress decrease of 8%.

Dumstorff et al. [25] analyzed stress increases due to inlays with a different elastic modulo. For inlays with lower modulo the authors show stress increases of up to 60%, especially in the corners of the surrounding material. The highest stress increase appearing in the edges is comparable to the notch effects observed in this contribution (see Figure 12). The stress increases found in this contribution are lower, this is mainly due to geometry: The rectangular edges used in the

FE models of Dumstorff et al. have sharper edges, leading to a higher stress increases.

Even though investigating another machine element, a comparison with Bonaiti et al. [35] is attempted. With their cavities on a gear they received 22% equivalent stress increase, which is in the same region as the results of Herbst et al. [34]. Hence, values around 20% seem like an overall compromise contributions are considering for the loss of mechanical function fulfillment for integrating sensors. The values in this contribution are in the same region.

### C. INTERPRETATION OF THE RESULTS

Regarding the **requirements for the sensor integration** posed in section I, the approach presented in this contribution helps to fulfill those. By choosing the location of the cavities for the sensors and electronics in the inside of the bolt, the standardized interfaces thread, head and outer dimensions are maintained. This ensures a wide and easy usage of the sensor integrating bolts and allow retrofitting. However, these cavities result in an impairment of the mechanical function (apply clamping forces), shown by the increase of the v. Mises stress. Every cavity, regardless of the location and size, will have this effect. This means that fulfilling the first two requirements to the full extent is exclusive: If the mechanical function must not be impaired, no cavities are allowed and the sensors have to be installed on the outside of the bolt, impairing the mechanical interfaces and outer dimensions. Hence, a decision has to be made in advance which way to follow.

The approach with the optimization function presented here helps to quantify the effect of the cavities on the mechanical function and also takes the new sensory function into account. Engineers are enabled to decide if the reduction of the mechanical function of the bolt is within boundaries. By knowing the exact forces acting on the bolt, a reduction of the security factor can be investigated, meaning that the mechanical function can be maintained.

In the scope of this contribution, **design space parameters** $d_1$, $d_2$, diameters of sensor and electronics cavity are varied, heights $h_1$, $h_2$ are fixed (see section II-C). This was argued with the high influence of the diameters on the stress and strain, and therefore on the mechanical and sensory fulfillment. Parameter $h_1$ will have a neglectable influence on stress or strain as long as it does not protrude in the thread area. Parameter $h_2$ however may have a higher influence. Since this part is predestined to house the electronics and energy buffer, varying this parameter will be necessary if more intelligence or longer run time without recharge is requested.

The **strain values at the shaft** are rather constant for $d_2$ when $d_1 \geq 8\,\text{mm}$ (see Figure 14). This leads to the conclusion that the effect of the design space parameter $d_2$, which is bolt's head housing the electronics, on the strain at the shaft is low. Given the locations, this seems reasonable.

**Comparison** of the **FE stress output** to **analytical equation**: Figure 15 shows the comparison of the analytical calculation with the FE model. The curves are close up until $d_1, d_2 \leq 16\,\text{mm}$. In this region these data points could even serve as input for the mechanical model, but only if normed and if $d_1 = d_2$. Setting up and running a FE-model is not necessary in that region. The discrepancies of $d_1, d_2 > 16\,\text{mm}$ can be explained by either simplifications made for the analytical equations or the fact that the FE model is based on data points for $0 \leq d_1 \leq 14\,\text{mm}$, and therefore out of that region not accurate anymore.

**Comparison** of the **FE strain output** to **strain gauge measurements** on test rig: There is an error between the FE-model output and the strain gauge measurements. This can have several reasons, as summarized below:

- Installment issues of the strain gauges (Glue issues, misalignment), which would explain the deviation in the absolute values as well as deviations in the slope.
- Tolerances of the mechanical structures of the clamping mechanisms, leading to bending loads on the strain gauges, see by the spacing of the individual strain gauge curves around the FE curve (Figures 18, 17).
- The strain gauge gives the mean of the strain below its measurement grid, which encompasses several points in the FE model.
- Offset and gain compensation was not accurate enough.

### D. LIMITATIONS

#### 1) EXAMPLE CASE M20 BOLT

The functions were parameterized using FE simulation outputs for a M20 bolt with shaft. Verification for other bolt sizes needs to be proven before this approach can be applied there.

#### 2) SENSOR BODY

The results from Figure 13 show that the sensor body reduces the maximum v. Mises stress because it shares the load. Thus, the mechanical function fulfillment index (MFI) increases. Though, this is only valid if the sensor body is made of a material with properties comparable to that of the bolt. In that case, the strain at the sensor position is reduced, reducing the sensory function fulfillment index (SFI). This highlights again the opposing objectives. To gain a higher SFI, the sensor body can be made of Aluminium or a polymer, with the cost of reducing the MFI. Considering that, the mounting of the sensor body needs to be reexamined.

#### 3) CURVE FITTING

The functions were fitted on certain data points from the FE outputs. Within these data points the error is small, as indicated by the $R^2$ values. However, outside these data points, especially for sensor cavity diameters $d_1, d_2 \geq 16\,\text{mm}$ there might be a higher error, also indicated by the deviation of the analytical and FE-model outputs from Figure 15. With an extended FE analysis this can be further improved.

### 4) MAXIMUM STRAIN IN SENSORY FUNCTION MODEL

The maximum strain of strain gauges, usually around 50 mm/m are currently neglected, but are also not touched by the solutions presented here. It can be taken into account by a penalty to the sensory function fulfillment part in the future.

### 5) BOUNDARY CONDITIONS AND WEIGHTS IN OPTIMIZATION FUNCTION

Boundary conditions are of great importance to the modelled functions. There are conditions that evolve from the sensor integration, e.g. $d_2 \geq d_1$. The location of the maxima is very much dependent on choosing the weights, as are the optimal design space parameters (see Figure 19. The weight factors resemble a prioritization of the function's parts. Therefore, in applications the prioritizing of the mechanical against the sensory functions has to be reasoned carefully.

### E. SUMMARY AND OUTLOOK

The research question posed in the introduction, *"How to overcome the conflict of objectives between the mechanical and sensory function fulfillment in identifying optimal design space parameters for force sensors?"*, is answered by this contribution. By finding evaluation criteria for mechanical and sensory function fulfillment and by modelling the effect of the design space parameters for the sensor integration on those function fulfillment, requirements from both the mechanical and sensory side can be taken into account to find optimal design space parameter sets. An optimization function could be composed which can be solved for minima, returning the optimal design space parameters.

Engineers of the involved disciplines mechanics and electronics are supported to balance how much design space each one gets by giving them data of the effects of the design space parameters. With that, this contribution discusses an approach for solving conflict of objectives regarding the design space of sensor integrating bolts in a standardized manner.

In the future, design space parameters that are fixed here will be varied to investigate their influence. Furthermore, other effects of the design space on the sensory function, next to the exploitation of the measuring range, are to be explored and integrated into the function. Ideas are to evaluate the space available for installment of more than one strain gauge for one measurement axis, giving the possibility to implement half- or full-bridge configurations.

Also, the approach of modelling the effects of the design space parameters to solve the conflicting objectives will be explored on other bolt sizes and other machine elements (other geometries and load cases) as well.

Furthermore, with the design space identified in this contribution a prototype of a sensor integrating M20 bolt with the sensor concept of [34] and the flexible modular electronics concept of [47] will be manufactured and subjected to static and dynamic testing. Communication of the acquired measurements to a host via standardized
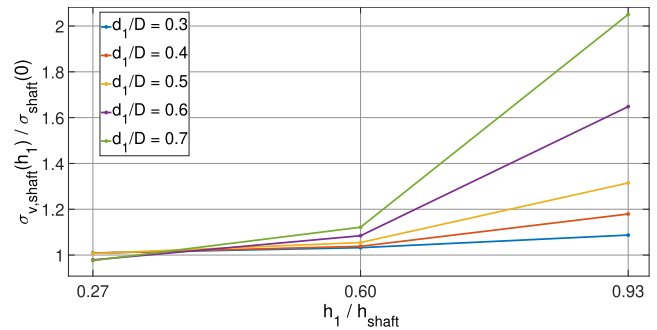


**FIGURE 22.** Influence of $h_1$ on stress $\sigma_{v,max}$ in notch shaft-thread, showing increases up to factor 2 depending on $d_1$.

protocols such as Bluetooth-Low-Energy (BLE) or Near-Field-Communication (NFC) will be of great concern, because the synchronization of data between the physical and the virtual world is key to enable digital twinning and perform predictive maintenance or fault diagnosis among others [12], [13].

### APPENDIX
### INVESTIGATION OF DESIGN SPACE PARAMETER HEIGHT

In order to investigate the influence of design space parameter $h_1$ on the v. Mises stress $\sigma_{v,max}$ a preliminary FE analysis was conducted, focusing the critical cross-sections at the notches head-shaft and shaft-thread. The results show a low influence of $h_1$ on $\sigma_{v,max}$ in the notch head-shaft. If $h_1$ protrudes in the cross-section of the notch shaft-thread, the $\sigma_{v,max}$ increases drastically (Figure 22). Hence, $h_1$ must not protrude in that cross-section.

### REFERENCES

[1] T. Kalsoom, N. Ramzan, S. Ahmed, and M. Ur-Rehman, "Advances in sensor technologies in the era of smart factory and Industry 4.0," *Sensors*, vol. 20, no. 23, p. 6783, Nov. 2020, doi: 10.3390/s20236783.

[2] Z. Liu and L. Zhang, "A review of failure modes, condition monitoring and fault diagnosis methods for large-scale wind turbine bearings," *Measurement*, vol. 149, Jan. 2020, Art. no. 107002, doi: 10.1016/j.measurement.2019.107002.

[3] F. Di Nuzzo, D. Brunelli, T. Polonelli, and L. Benini, "Structural health monitoring system with narrowband IoT and MEMS sensors," *IEEE Sensors J.*, vol. 21, no. 14, pp. 16371–16380, Jul. 2021, doi: 10.1109/JSEN.2021.3075093.

[4] M. L. Wymore, J. E. Van Dam, H. Ceylan, and D. Qiao, "A survey of health monitoring systems for wind turbines," *Renew. Sustain. Energy Rev.*, vol. 52, pp. 976–990, Dec. 2015, doi: 10.1016/j.rser.2015.07.110.

[5] S. Nandi, H. A. Toliyat, and X. Li, "Condition monitoring and fault diagnosis of electrical motors—A review," *IEEE Trans. Energy Convers.*, vol. 20, no. 4, pp. 719–729, Dec. 2005, doi: 10.1109/TEC.2005.847955.

[6] Q. Bian, C. Bauer, A. Stadler, M. Lindner, M. Jakobi, W. Volk, A. W. Koch, and J. Roths, "In-situ high temperature and large strain monitoring during a copper casting process based on regenerated fiber Bragg grating sensors," *J. Lightw. Technol.*, vol. 39, no. 20, pp. 6660–6669, Oct. 2021, doi: 10.1109/JLT.2021.3101524.

[7] E. Kirchner, G. Martin, and S. Vogel, "Sensor integrating machine elements: Key to in-situ measurements in mechanical engineering," in *Proc. 23rd Seminário Internacional de Alta Tecnologia*, 2018, pp. 1–10.

[8] P. Groche, J. Hohmann, and D. Übelacker, "Overview and comparison of different sensor positions and measuring methods for the process force measurement in stamping operations," *Measurement*, vol. 135, pp. 122–130, Mar. 2019, doi: 10.1016/j.measurement.2018.11.058.

[9] F. Bleicher, C. Ramsauer, M. Leonhartsberger, M. Lamprecht, P. Stadler, D. Strasser, and C. Wiedermann, "Tooling systems with integrated sensors enabling data based process optimization," *J. Mach. Eng.*, vol. 21, no. 1, pp. 5–21, Mar. 2021, doi: 10.36897/jme/134244.

[10] G. Martin, S. Vogel, T. Schirra, G. Vorwerk-Handing, and E. Kirchner, "Methodical evaluation of sensor positions for condition monitoring of gears," in *Proc. NordDesign*, P. Ekströmer, S. Schütte, and J. Ölvander, Eds., Linköping, Sweden: Univ. of Linköping, Aug. 2018.

[11] K. Hofmann, F. Keil, S. Matthiesen, T. Gwosch, M. Kupnik, E. Kirchner, D. Göhringer, M. Otto, and K. Stahl, "Potenziale und Herausforderungen Energieautonomer Sensorsysteme Für den Einsatz in sensorintegrierenden Maschinenelementen," in *EASS*, O. Schecker, Ed. Hessen, Germany: VDE Verlag GmbH, 2022, pp. 36–38.

[12] A. Thelen, X. Zhang, O. Fink, Y. Lu, S. Ghosh, B. D. Youn, M. D. Todd, S. Mahadevan, C. Hu, and Z. Hu, "A comprehensive review of digital twin—Part 1: Modeling and twinning enabling technologies," *Struct. Multidisciplinary Optim.*, vol. 65, no. 12, p. 354, Dec. 2022, doi: 10.1007/s00158-022-03425-4.

[13] D. Jones, C. Snider, A. Nassehi, J. Yon, and B. Hicks, "Characterising the digital twin: A systematic literature review," *CIRP J. Manuf. Sci. Technol.*, vol. 29, pp. 36–52, May 2020, doi: 10.1016/j.cirpj.2020.02.002.

[14] E. Kirchner et al., "A review on sensor-integrating machine elements," *Adv. Sensor Res.*, vol. 3, no. 4, pp. 2300113–2300150, Apr. 2024, doi: 10.1002/adsr.202300113.

[15] N. Hendrich, F. Wasserfall, and J. Zhang, "3D printed low-cost force-torque sensors," *IEEE Access*, vol. 8, pp. 140569–140585, 2020, doi: 10.1109/ACCESS.2020.3007565.

[16] G. Vorwerk-Handing, T. Gwosch, S. Schork, E. Kirchner, and S. Matthiesen, "Classification and examples of next generation machine elements," *Forschung IM Ingenieurwesen*, vol. 84, no. 1, pp. 21–32, Mar. 2020, doi: 10.1007/s10010-019-00382-1.

[17] *DFG Priority Programme 2305: Sensor Integrating Machine Elements: Enablers for Comprehensive Digitization*, German Res. Found., Bonn, Germany, 2020.

[18] W. Steinhilper and B. Sauer, *Konstruktionselemente des Maschinenbaus 1*. Berlin, Germany: Springer, 2012.

[19] P. Groche and M. Brenneis, "Manufacturing and use of novel sensoric fasteners for monitoring forming processes," *Measurement*, vol. 53, pp. 136–144, Jul. 2014, doi: 10.1016/j.measurement.2014.03.042.

[20] *ISO General Purpose Metric Screw Threads—Part 1: Nominal Sizes for Coarse Pitch Threads; Nominal Diameter From 1 mm to 68 mm*, document DIN 13-1:1999-11, 1999, doi: 10.31030/8133800.

[21] *Fasteners Hexagon Head Bolts Product Grades A and B*, document DIN EN ISO 4014, Oct. 2022, doi: 10.31030/3279821.

[22] *Systematic Calculation of Highly Stressed Bolted Joints, Joints With One Cylindrical Bolt*, document VDI 2230 Blatt 1, Beuth Verlag GmbH, Nov. 2015.

[23] B. Blachowski and W. Gutkowski, "Effect of damaged circular flange-bolted connections on behaviour of tall towers, modelled by multilevel substructuring," *Eng. Struct.*, vol. 111, pp. 93–103, Mar. 2016, doi: 10.1016/j.engstruct.2015.12.018.

[24] J. Peters, C. Zimmerer, T. Gwosch, F. Herbst, C. Hartmann, R. Chadda, D. Riehl, F. Keil, M. Kupnik, and K. Hofmann, "Test-driven development to overcome challenges in the design of sensor-integrating machine elements," in *Proc. DS 119 33rd Symp. Design X (DFX)*, 2022, p. 10, doi: 10.35199/dfx2022.12.

[25] G. Dumstorff, S. Paul, and W. Lang, "Integration without disruption: The basic challenge of sensor integration," *IEEE Sensors J.*, vol. 14, no. 7, pp. 2102–2111, Jul. 2014, doi: 10.1109/JSEN.2013.2294626.

[26] J. Mihm, C. Loch, and A. Huchzermeier, "Problem–solving oscillations in complex engineering projects," *Manage. Sci.*, vol. 49, no. 6, pp. 733–750, Jun. 2003.

[27] T. Frank, A. Grün, M. Kermann, A. Cyriax, A. Steinke, T. Ortlepp, and G. Reschke, "2.2.4 hybridintegration von mikrodehnungssensoren," in *Proc. GMA/ITG-Fachtagung Sensoren und Messsysteme*, 2019, pp. 153–158, doi: 10.5162/sensoren2019/2.2.4.

[28] S. Biehl, N. Paetsch, E. Meyer-Kornblum, and G. Bräuer, "Wear resistenat thin film sensor system for industrial applications," *Int. J. Instrum. Meas.*, vol. 1, pp. 6–11, Jan. 2016.

[29] Fraunhofer Institute for Surface Engineering and Thin Films IST. (2022). *Smart Screw Connection—Wireless and Energy-Autonomous Monitoring Solution*. [Online]. Available: https://www.ist.fraunhofer.de

[30] ConSenses GmbH. (2023). *Zeitgemaße Industriemesstechnik Smarte Lösungen | ConSenses Industrial Intelligence*. [Online]. Available: https://consenses.de/en/home

[31] M. Brenneis and P. Groche, "Integration of piezoceramic tube under prestress into a load carrying structure," *Adv. Mater. Res.*, vols. 966–967, pp. 651–658, Jun. 2014.

[32] ConSenses GmbH. (2016). *Montageanleitung PiezoBolt PB und Signalleitung LC*. [Online]. Available: https://consenses.de.

[33] Core Sensing GmbH. (2024). *coreIN Sensor Integration*. [Online]. Available: https://core-sensing.de/en/produktgruppe/sensoren/corein/

[34] F. Herbst, R. Chadda, C. Hartmann, J. Peters, D. Riehl, T. Gwosch, K. Hofmann, S. Matthiesen, and M. Kupnik, "Multi-axis force sensor for sensor-integrating bolts," in *Proc. IEEE Sensors*, Oct. 2022, pp. 1–4, doi: 10.1109/SENSORS52175.2022.9967220.

[35] L. Bonaiti, E. Knoll, M. Otto, C. Gorla, and K. Stahl, "The effect of sensor integration on the load carrying capacity of gears," *Machines*, vol. 10, no. 10, p. 888, Oct. 2022, doi: 10.3390/machines10100888.

[36] D. Großkurth and G. Martin, "Intelligenter Zahnriemen," in *Proc. GMA/ITG-Fachtagung Sensoren und Messsysteme*, 2019, pp. 738–743, doi: 10.5162/sensoren2019/P2.14.

[37] J. S. Gero, "A knowledge representation schema for design," *AI Mag.*, 1990, doi: 10.1609/aimag.v11i4.854.

[38] J. S. Gero and U. Kannengiesser, "The function-behaviour-structure ontology of design," in *An Anthology of Theories and Models of Design*, A. Chakrabarti and L. T. M. Blessing, Eds. London, U.K.: Springer, 2014, pp. 263–283, doi: 10.1007/978-1-4471-6338-1_13.

[39] S. Matthiesen, "Gestaltung—Prozess und methoden," in *Pahl/Beitz Konstruktionslehre*, B. Bender and K. Gericke, Eds. Berlin, Germany: Springer, 2021, pp. 397–465, doi: 10.1007/978-3-662-57303-7_13.

[40] J. Peters and S. Matthiesen, "Procedure to identify optimal design space for integration of sensors into machine elements," Repository KITopen, Karlsruhe, Germany, Tech. Rep. 1000169793, 2024, doi: 10.5445/IR/1000169793.

[41] R. C. Hibbeler, *Technische Mechanik 2—Festigkeitslehre (Mechanics of Materials)*, vol. 4409. München, Germany: Pearson, 2021.

[42] *Calculation of Load Capacity of Shafts and Axles—Part 2: Theoretical Stress Concentration Factors and Fatigue Notch Factors*, document DIN 743-2, Dec. 2012, doi: 10.31030/1818282.

[43] J. Montgomery, "Boundary condition influences on shank stress in 3D solid bolt simulation," in *Proc. Abaqus Users' Conf.*, 2008, pp. 19–22.

[44] K. Hofmann. *Applying the Wheatstone Circuit, Hottinger Baldwin Messtechnik (HBM)*. [Online]. Available: https://www.hbm.com/fileadmin/mediapool/hbmdoc/technical/T01569.pdf

[45] K. Hofmann. *An Introduction to Stress Analysis using Strain Gauges, Hottinger Baldwin Messtechnik (HBM)*. [Online]. Available: https://www.hbm.com

[46] M. A. Sahib and B. S. Ahmed, "A new multiobjective performance criterion used in PID tuning optimization algorithms," *J. Adv. Res.*, vol. 7, no. 1, pp. 125–134, Jan. 2016, doi: 10.1016/j.jare.2015.03.004.

[47] D. Riehl, D. Korner, F. Keil, J. Peters, S. Matthiesen, and K. Hofmann, "Flexible modular electronic platform for sensor-integrating bolts," in *EBL 2024: Elektronische Baugruppen und Leiterplatten*, vol. 107. Frankfurt, Germany: GMM-Fachbericht, VDE-Verlag, 2024, pp. 313–316.

**JULIAN PETERS** received the M.Sc. degree in mechatronics and information technology from Karlsruhe Institute of Technology (KIT), Karlsruhe, in 2020, where he is currently pursuing the Ph.D. degree. During his studies, he did student jobs in and out of Germany dealing with automation solutions using industrial robots and prototyping for assembly lines, among others. Since 2020, he has been a Researcher with KIT, focused on methodically integrating sensors into machine elements to gain insight in health states and processes of machines and support comprehensive digitization.

**NATHANAEL MIRBACH** is currently pursuing the bachelor's degree in mechanical engineering with Karlsruhe Institute of Technology (KIT). During an internship, he worked in the development of autonomous robots used in production. In 2023, he worked with Julian Peters on the integration of sensors into bolts, for the bachelor's thesis. He has conducted CAE analyses, manufactured test specimen, and supported in verification.

**FELIX HERBST** (Student Member, IEEE) received the M.Sc. degree in electrical engineering from Technische Universität (TU) Darmstadt, Germany, in 2022. Since then, he has been a Research Associate with the Measurement and Sensor Technology Group, TU Darmstadt. His research interests include the design of structural integrated mechanical sensors and robotics in medical applications.

**DAVID RIEHL** (Student Member, IEEE) received the M.Sc. degree in electrical engineering from the Technische Universität (TU) Darmstadt, Germany, in 2020. Since then, he has been a Research Associate with the Integrated Electronic Systems Laboratory, TU Darmstadt. His research interests include the integration of electronics into machine elements, with a focus on power supply and communication and interconnect modeling and system test.

**MARIO KUPNIK** (Senior Member, IEEE) received the Diplom-Ingenieur degree in electrical engineering from Graz University of Technology, Austria, in 2000, and the Ph.D. degree in electrical engineering from the University of Leoben, Leoben, Austria, in 2004. From 2005 to 2011, he was a Postdoctoral Researcher, a Research Associate, and a Senior Research Scientist with the Edward L. Ginzton Laboratory, Stanford University, Stanford, CA, USA. From 2011 to 2014, he was a Full Professor of electrical engineering with the Brandenburg University of Technology, Cottbus, Germany. Since 2015, he has been a Full Professor with the Technische Universität Darmstadt, Germany, where he is currently the Head of the Measurement and Sensor Technology Group. His research interests include micromachined sensors and actuators, multiphysics simulations, ferroelectrets, flowmetering of gases and liquids, ultrasound, electroacoustics, human–machine interaction, and robotics.

**KLAUS HOFMANN** (Senior Member, IEEE) received the Engineer (Diplom-Ingenieur) degree in electrical engineering from Ruhr University Bochum, Germany, in 1992, and the Dr.-Ing. degree from TU Darmstadt, in 1997. From 1998 to February 2009, he was with Siemens AG, Infineon Technologies AG, and Qimonda AG, in various positions (last position: the Director of Product Development), such as leading the Advanced Technology Software and the Product Development Department, designing DDR-DDR3 DRAM products ranging from 90nm down to 65nm technologies. Since 2009, he has been leading the Integrated Electronic Systems Laboratory, TU Darmstadt, as a Full Professor. His research interests include analog and digital integrated circuits and systems, application of integrated circuits in robust environments (mechanical engineering and the IoT), and novel devices, such as memristors and RFETs.

**SVEN MATTHIESEN** received the Engineer (Dipl.-Ing.) degree in mechanical engineering and the Ph.D. degree from University Karlsruhe (TH, currently KIT), in 1997 and 2002, respectively. He was with HILTI, Liechtenstein, from 2003 to 2010, as a Design Engineer for power tools and the Head of development for screw technology. He is the Head of the Institute of Product Engineering, KIT, and has a professorship for power tools and machine elements, since 2010. His research interests include mechatronization of machine elements, design methods to support engineers, power tools, and human–machine interaction.

• • •